Change of chemical bonding properties at SiN_x/GaN/AlGaN interface with SiH_4 flow rate and its impact on the carrier transport properties of MIS-diodes

Pradip Dalapati,[a,*] Subramaniam Arulkumaran,[b] Dinesh Mani,[a] Hanchao Li,[a] Hanlin Xie,[c,d] Yue Wang,[e] Geok Ing Ng[a,b,c,d,e]

[a]*School of Electrical and Electronic Engineering, Nanyang Technological University, 50 Nanyang Avenue, Singapore 639798, Singapore*

[b]*Temasek Laboratories@NTU, Nanyang Technological University, Research Techno Plaza, 50 Nanyang Drive, Singapore 637553, Singapore*

[c]*Institute of Microelectronics (IME), Agency for Science, Technology and Research (A*STAR), 2 Fusionopolis Way, Innovis #08-02, Singapore 138634, Singapore*

[d]*National GaN Technology Centre (NGTC), Agency for Science, Technology and Research (A*STAR), 2 Fusionopolis Way, Innovis #08-02, Singapore 138634, Singapore*

[e]*Low Energy Electronic Systems (LEES) Plus, Singapore-MIT Alliance for Research and Technology Centre, 1 CREATE Way, #10-01 CREATE Tower, Singapore 138602, Singapore*

[*]Corresponding author. *E-mail address:* pradipdalapati@gmail.com (P. Dalapati)

ABSTRACT

The understanding of the properties of silicon nitride (SiN_x) deposited by plasma-enhanced chemical vapor deposition (PECVD) is crucial as this layer is widely used for gate dielectric and surface passivation. In the PECVD system, the passivation quality can be altered substantially with SiH_4 flow rate. Therefore, in the present work, variation of chemical structures at the SiN_x/GaN interface with SiH_4 flow rate and its impact on the charge transport mechanisms of metal-insulator-semiconductor (MIS) diodes have been systematically investigated. X-ray photoelectron spectroscopy results suggest that the trap states related to Ga-O and N-H bonds decline when SiH_4 flow rate increases from 55 to 85 sccm, leading to a reduction of surface-electron trapping and an improvement in surface passivation quality. The same observation can also be confirmed using Fourier transform infrared spectroscopy measurements. The leakage current and interface trap density of MIS-diode with 85 sccm SiH_4 flow rate deposited SiN_x are significantly lower than that of MIS-diode with 55 sccm SiH_4 flow rate deposited SiN_x. Interestingly, after passivation, the density of slow traps is suppressed largely and we achieved a minimum interface trap density of 1.57×10^{12} $cm^{-2}.eV^{-1}$ which helps to suppress three orders of magnitude lower leakage current compared to the conventional Schottky diode.

Keywords: AlGaN/GaN, PECVD SiN_x, Chemical bonds, Interface states, Carrier trapping.

1. Introduction

It is well known that the existence of a large number of surface states in AlGaN/GaN-based power devices can play a strong detrimental role in their DC and RF performances [1-6]. The effect becomes more significant for the device fabricated with lower AlGaN barrier layer thickness, where the surface charge-related electrostatic effect could be increased on the free carriers confined in the channel region due to the shorter distance between the two-dimensional electron gas (2DEG) and the surface of heterostructure [1].

The origin of surface states in GaN-based semiconductor materials could be related to the oxygen impurities, threading dislocations, dangling bonds, and nitrogen vacancies as suggested in Refs. [7-10]. These defect states can play various roles in many unfavorable effects in metal/AlGaN/GaN-based conventional Schottky diodes (MS-diodes). The conventional MS-diodes without surface passivation have unacceptably high reverse leakage current due to the presence of several surface states [8,9]. It is reported that the large number of surface states in conventional MS-diodes could make 2DEG at the AlGaN/GaN interface difficult to deplete [7,8]. Many reports also highlighted the surface states-related Fermi level (E_F) pinning effects in conventional MS-diodes [7,8]. The Fermi level pinning can limit the work function dependence of the Schottky barrier height and worsen the device performance [7].

However, different oxide (e.g., Al_2O_3, HfO_2, and SiO_2) or nitride (e.g., SiN and AlN) based dielectric films have been used to mitigate the negative effects of surface states [11-13]. Several researchers have used SiN_x dielectric layer, commonly deposited with a plasma-enhanced chemical vapor deposition (PECVD) system, for surface passivation as SiN_x provides additional positive charges to neutralize the previously trapped negative electrons on the surface states thanks to the unique property of SiN_x [2,14,15]. However, several oxide states and dangling bonds at the interface between SiN_x and GaN remain a source of carrier trapping and thus hinder the device performance [2]. Lu et al. have noticed that after PECVD SiN_x passivation, the interface state density (D_{it}) decreases from about 4.54×10^{12} $cm^{-2}eV^{-1}$ (un-passivated) to 1.96×10^{12} $cm^{-2}eV^{-1}$ at 0.328 eV of relative trap level below conduction band which improves the device performance [16]. In addition, the gate leakage current can be suppressed considerably in the metal-insulator-semiconductor high-electron-mobility transistors (MIS-HEMTs) by using the low-temperature-grown SiN_x as gate dielectric and passivation layers as suggested by Surana et al. [11]. A similar observation can also be found in Ref. [17] where the authors claimed that after the inclusion of a passivation layer, the device performance improves in terms of lower gate leakage current and better pinch-off characteristics.

Furthermore, it is noted that the surface state filling closely depends on the chemical bonds between SiN_x and GaN surfaces [18]. Therefore, to suppress the dielectric trapping and interface states at the SiN_x/GaN interface, a better understanding of the chemical bonding properties of SiN_x is required. The chemical structures of SiN_x can largely alter with the deposition parameters (e.g., plasma power density, temperature, pressure, and flow rate of gas precursors) in the PECVD system [18,19]. The change of chemical structures in SiN_x can affect the surface passivation quality substantially as found in [18,19].

Several research groups used different gas flow rates for the deposition of SiN_x in the PECVD process to control the trapping of surface-electrons and improve the device performance [3,4,19,20]. However, the combined effects of gas flow rate on the chemical structures formed between the gate dielectric layer and GaN and its modifications after the deposition of a thick passivation layer are not well studied. Therefore, the change of chemical structures with the gas flow rate during the deposition of gate dielectric and passivation layers and its effect on the carrier transport mechanisms of metal-insulator-semiconductor-based devices should be investigated thoroughly.

Before going to describe the work in detail, certain key features of the study are mentioned below. First, we deposited the SiN_x gate dielectric layers on the GaN/AlGaN/AlN/GaN epilayer at two different gas (SiH_4/NH_3) flow rates in the PECVD system. Second, we have investigated the chemical bonding properties at the SiN_x/GaN/AlGaN interfaces for both samples by analyzing the X-ray photoelectron spectroscopy (XPS) and Fourier transform infrared (FTIR) spectra. Third, to investigate the effect of SiH_4/NH_3 flow rate on the carrier transport mechanisms, we have measured the current–voltage (I–V), capacitance–voltage (C–V), and parallel conductance–radial frequency (G_p–ω) characteristics in the fabricated MIS-diodes. Based on the obtained results, we have examined two distinct interface trapping regions (slow and fast traps) with different values of interface state density and thus elucidated the effect of slow and fast traps on the leakage current (I_{leak}) processes (e.g., trap-assisted tunneling) and the capacitance profile of the device. Fourth, to reduce the values of I_{leak}, and D_{it} further, we have fabricated another two samples with MIS-diodes by utilizing the thick passivation layers. Fifth and finally, we have highlighted the importance of the thick passivation layer to improve the interface quality through the suppression of interface states, especially the slower traps.

2. Experimental

Figure 1 shows the schematic cross-section of the MIS-diodes where the main III-nitride materials (GaN/AlGaN/AlN/GaN) were grown by the metal organic chemical vapor deposition (MOCVD) system. The heterostructures exhibited an electron mobility of 1775 cm^2/Vs, a sheet resistance of 389 Ω/□, and a 2DEG sheet carrier density of 8.97×10^{12} cm^{-2} at room temperature (RT) as confirmed via Hall measurement.

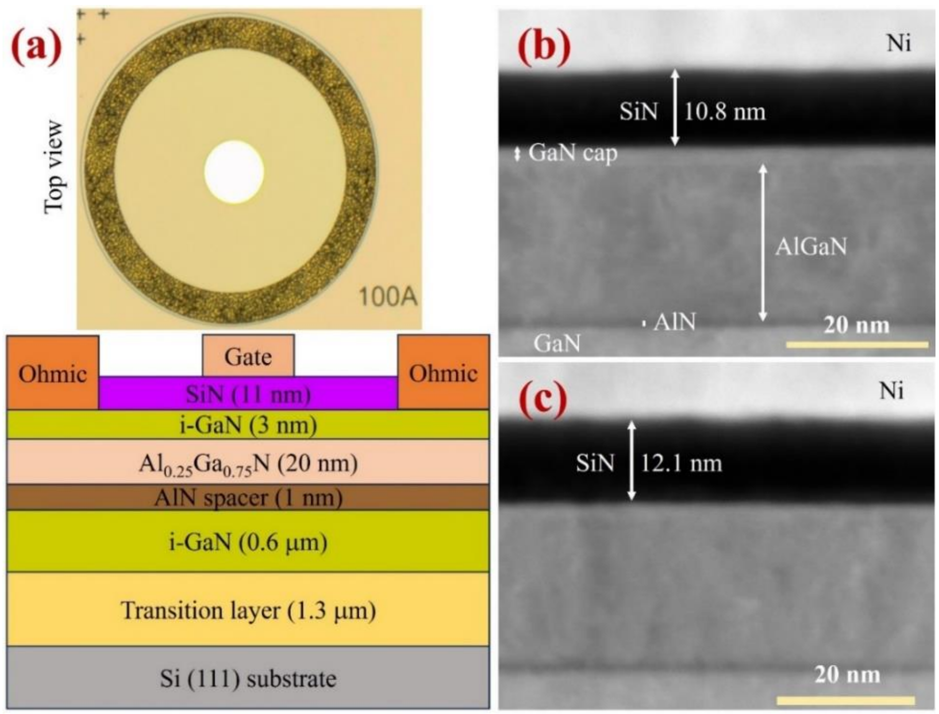

Fig. 1. Schematic cross-section of SiN_x/GaN/AlGaN/AlN/GaN MIS-diode with the image of top view (a). (b) and (c) the cross-sectional STEM images under the gate region of samples A and B, respectively.

The device fabrication process was started with the mesa isolation step by the inductively-coupled-plasma reactive ion etching (ICP-RIE) using BCl_3 and Cl_2 gas chemistry. Next, the Ohmic metal stacks of Ti/Al/Ni/Au (20/120/40/50 nm) were deposited by the electron beam evaporation (EBE) process. To achieve an excellent ohmic contact, a rapid thermal annealing process at 800

°C for 30 s in the N_2 atmosphere was conducted. After that, the transmission line measurement (TLM) was carried out to measure the contact resistance (R_c) of the formed ohmic contact. The TLM was carried out with an Agilent E5270B analyzer at RT. The samples exhibited an average R_c of 0.38 Ω-mm at RT. However, after the formation of ohmic contact, the SiN_x insulating layer of about 11 nm was deposited by the PECVD process at 300 °C. In this work, two different types of SiN_x layers were deposited by changing the SiH_4 flow rate from 55 (sample A) to 85 (sample B) sccm, while the NH_3 flow rate (= 145 sccm) and all the deposition parameters (plasma power and pressure) were preserved constantly. Similar PECVD-SiN_x layers with SiH_4 flow of 55 and 85 sccm were deposited on Si substrate for the ellipsometry measurements. The spectroscopic ellipsometry (J.A. Woollam, M-2000® Spectroscopic Ellipsometer) measurements were performed to evaluate the refractive index and thickness of the deposited SiN_x films. The M-2000-based spectroscopic ellipsometer with 30 W of Deuterium light source was mounted on the auto-angle system (ESM base), where we can vary the step angle at different degrees. The measurements were performed at different incidence angles from 55° to 75° (step angle = 5°).

After confirmation of the required thickness of the deposited PECVD-SiN_x, the gate metal stacks of Ni/Au (50/250 nm) were then deposited by electron beam evaporation followed by a lift-off process. To study the influence of passivation, a thick PECVD-SiN_x layer (~130 nm) was deposited just after the formation of gate contact. Two different types of PECVD-SiN_x passivation layers were deposited at 300 °C by changing the SiH_4 flow rate from 55 to 85 sccm. However, the flow rate of NH_3 (= 145 sccm) and all the deposition parameters (plasma power and pressure) were maintained constantly during the deposition of SiN_x passivation layers. Finally, to remove the SiN_x layer from the top of Ohmic and gate contact pads, a CF_4/CHF_3 gas mixture based RIE process was conducted. In this work, the fabricated un-passivated MIS-diodes were designated as MIS-diode A (SiH_4 flow = 55 sccm for the deposition of SiN_x gate insulation) and MIS-diode C (SiH_4 flow = 85 sccm for the deposition of SiN_x gate insulation), while the passivated MIS-diodes were defined as MIS-diode B (SiH_4 flow = 55 sccm for the deposition of SiN_x gate insulation and passivation layer) and MIS-diode D (SiH_4 flow = 85 sccm for the deposition of SiN_x gate insulation and passivation layer).

The thickness of the deposited SiN_x layers (t_{SiN}) was estimated from the cross-sectional scanning transmission electron microscopy (STEM) image (Figs. 1(b) and 1(c)). The obtained values of t_{SiN} for samples A and B were 10.8 and 12.1 nm, respectively. The obtained values of t_{SiN} are slightly higher than the designed value. This is ascribed to the variation of deposition rate in different degrees with the SiH_4 flow rates. However, all the device characterizations (*I*–*V*, *C*–*V*, and G_p–ω) were carried out by using a power device analyzer (Agilent B1505A). The power device analyzer was connected to a high-voltage probe station under an electrically shielded condition. Before *C*–*V*, and G_p–ω measurements, the capacitance measurement unit in the power device analyzer was calibrated by conducting the open and short corrections in sequence order. In addition, it is to be mentioned that in the present investigation, all the device characterizations were performed at room temperature.

3. Results and discussion

3.1. Ellipsometer measurement

We have investigated the effect of SiH_4 flow rate on deposition rate and refractive index of SiN_x by employing spectroscopic ellipsometry. The wavelength-dependent refractive index $n(\lambda)$ and extinction coefficient $k(\lambda)$ of the SiN_x layer are evaluated by the Tauc-Lorentz models in 245.5 to 1688 nm (photon energy = 0.73 to 5 eV) range and the obtained results are shown in Fig. 2. The deposition rate of PECVD-SiN_x increases from 1.11 nm/sec to 1.15 nm/sec when the SiH_4 flow increases from 55 (sample A) to 85 (sample B) sccm. The increase in the deposition rate of SiN_x is attributed to the availability of a large number of reactive Si species for the deposition [21]. The higher SiH_4 flow can increase (decrease) the proportion of SiH_x (NH_y) radicals in the reactor chamber, leading to a higher deposition rate and higher value of silicon-to-nitrogen (Si/N) ratio in the film [22]. A similar observation can also be noticed in Refs. [21,22]. However, the high SiH_4 flow rate could lead to an increase in Si-Si and Si-H bonds which in the end increase the light absorption in SiN_x film. It is noticed in Fig. 2 (b) that the value of k (imaginary part of the complex optical index $N_{op} = n + ik$) in sample B is higher even at lower photon energy, indicating the improvement of Si-Si absorbing bonds [23,24].

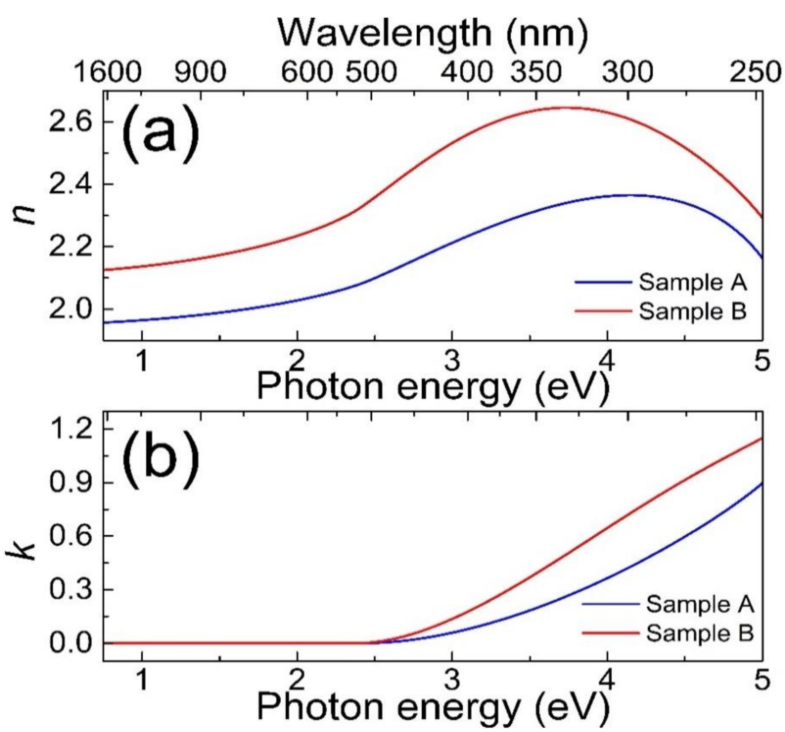

Fig. 2. (a) Refractive index and (b) extinction coefficient of sample A (SiH_4 flow = 55 sccm), and sample B (SiH_4 flow = 85 sccm).

It should be noted that the extinction coefficient can change the refractive index of the film as it is closely related to the refractive index [23]. When the SiH_4 flow rate increases from 55 to 85 sccm (Si/N ratio increases from 1.74 to 2.36; we describe the detail in section 3.3), *n* increases from 2.05 (sample A) to 2.26 (sample B), suggesting the dominance of Si-Si absorbing bonds. A similar effect of SiH_4 flow rate on the refractive index of PECVD-SiN_x has been reported in Refs. [21,23-25]. The authors in Ref. [26] noticed that when SiH_4/NH_3 ratio increases from 0.05 to 3, *n* increases from 1.81 to 2.52. In another work, Lelievre et al. [24] suggested that the value of *n* increases from 1.98 to 2.98 when the Si/N ratio changes from 0.7 to 2.86, validating the finding of our present work.

3.2. Fourier transform infrared spectroscopy analysis of PECVD-SiNx

In order to shed more light on the effect of SiH_4 flow rate on different chemical structures in PECVD-SiN_x film and its surface passivation quality, we have performed the Fourier transform infrared spectroscopy under transmission mode. The measured FTIR spectra of both SiN_x films (samples A and B) from 400 to 4000 cm^{-1} are shown in Fig. 3.

For the surface passivation of GaN, SiN_x film with higher N-H bonds is inferior to Si-H bonds as claimed in [27,28]. N-H bonds in SiN_x act as the precursors of K^+ centers and increase the interface trap density [27,29]. On the other hand, the formation of Si-H bonds in SiN_x can neutralize the deep interface states effectively and thus reduce the value of D_{it} as reported in Refs. [3,24,27]. Henceforth, to improve surface passivation and device performance by minimizing D_{it}, the reduction (improvement) of N-H (Si-H) bonds in SiN_x film is essential.

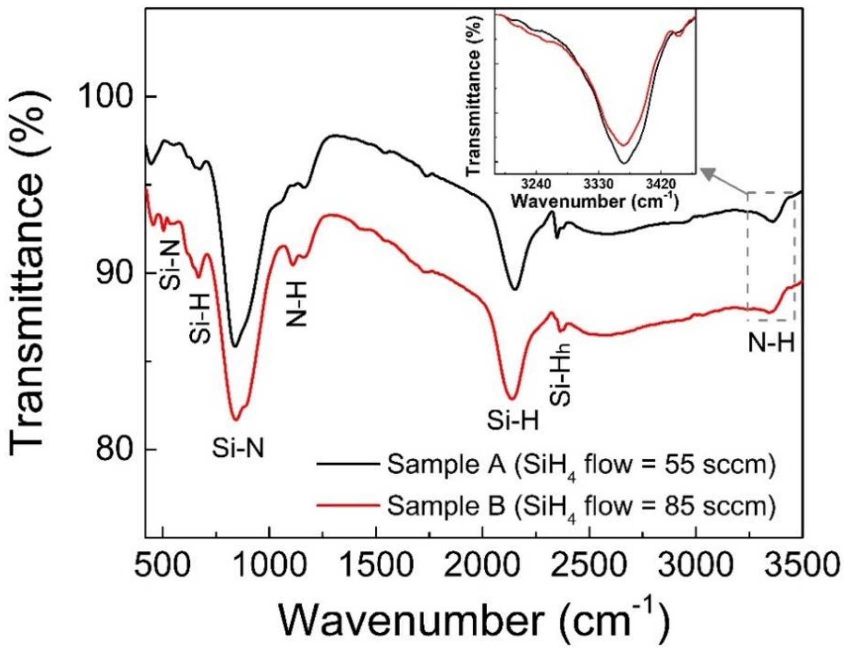

Fig. 3. FTIR transmission spectra of PECVD-SiN_x at RT. Inset: A magnified view of the peaks at 3362 cm^{-1}, where the baselines of the peaks are adjusted to the same height by the Shirley baseline correction method.

The FTIR spectra exhibit Si-N (asymmetric), Si-H, and N-H stretching modes at 844, 2138, and 3362 cm^{-1}, respectively (see Fig. 3). The small peaks at 456, 650, 1110, and 2370 cm^{-1} could be attributed to the Si-N symmetric stretching mode [30], Si-H, and N-H wagging modes [30,31], and hydride stretching mode of Si-H (Si-H_h) [32], respectively. It is noticed in Fig. 3 that with an increase in the SiH_4 content (sample B), the transmittance peak at 3362 cm^{-1} decreases slightly. A magnified view of the transmittance peaks at 3362 cm^{-1} is shown in the inset of Fig. 3, where the baselines of both peaks are adjusted to the same level by the Shirley baseline correction method for a better comparison. The decrease in transmittance peak at 3362 cm^{-1} indicates that the formation of N-H bonds declines slightly due to higher SiH_4 flow [26]. On the other hand, the transmittance peak at 2138 cm^{-1} increases in sample B. This increase in transmittance peak at 2138 cm^{-1} is attributed to the enhanced Si-H chemical bonds. The SiN_x film with stronger Si-H bonds will improve the SiN_x/GaN interface by mitigating the formation of deep-level surface traps which leads to reduce the electron-hole recombination process greatly by field-effect passivation [23,24,26,33,34]. In addition, based on this observation, we believe that the higher SiH_4 flow rate will help to reduce the reverse leakage current (I_{leak}) and interface trap density in the fabricated device (which we describe in sections 3.4 and 3.6).

3.3. Evaluation of the stoichiometry of SiN_x from X-ray photoelectron spectroscopy analysis

To study the insight of stoichiometry (Si/N) of PECVD-SiN_x films (cleaned surface of the film having thickness greater than 130 nm) and chemical bonding states at SiN_x/GaN/AlGaN interfaces, we have performed X-ray photoelectron spectroscopy (X-ray source: Al Kα radiation, X-ray power: 225 W) in a high vacuum environment. It should be mentioned that all the acquired XPS spectra (wide and narrow scans) in the present investigation are adjusted by the C 1s peak at 284.8 eV. The wide survey spectra of XPS for samples A and B are displayed in Fig. 4, where all the dominated peaks at various binding energies are marked clearly. Moreover, to reach the SiN_x/GaN/AlGaN interfaces, we have etched down the SiN_x films via Ar^+ ion etching until the appearance of Al signal from the underneath AlGaN barrier layer. Noted, the values of Al peaks in samples A and B are almost the same. Here, we have carried out the etching process by using an Ar Gas Cluster Ion Source (Kratos Analytical Inc. Mini-beam 6) operated at 5 keV Ar^+ (raster size = 2×2 mm^2) with the optimized eating rate (for say, 5.8 nm per minute for sample A).

The survey spectra obtained at the SiN_x/GaN/AlGaN interfaces contain some additional GaN-related peaks marked in Fig. 4 (see blue lines). Interestingly, due to the appearance of different GaN-related XPS peaks, the spectra at the interface are dissimilar from the as-deposited bulk SiN_x spectra, suggesting that the chemical bonds at the interface are altered. Therefore, the analysis of the change of chemical bonds at the interface is necessary, which we discuss separately.

However, to evaluate the value of Si/N ratio, we acquired the wide survey spectra from the bulk SiN_x films. Due to higher silane content, the value of Si/N in sample B (2.36) is higher than that of sample A (1.74). The higher value of Si/N ratio indicates the presence of excess silicon in sample B, where the excess silicon has a greater influence on the refractive index as noticed in the ellipsometry measurement. Furthermore, the obtained bandgap (E_g) by reflection electron energy loss spectroscopy (REELS) of sample A (lower Si/N ratio) and B (higher Si/N ratio) are about 5.45 and 3.85 eV, respectively, which are consistent with the E_g values reported by Nguyen et al. [26].

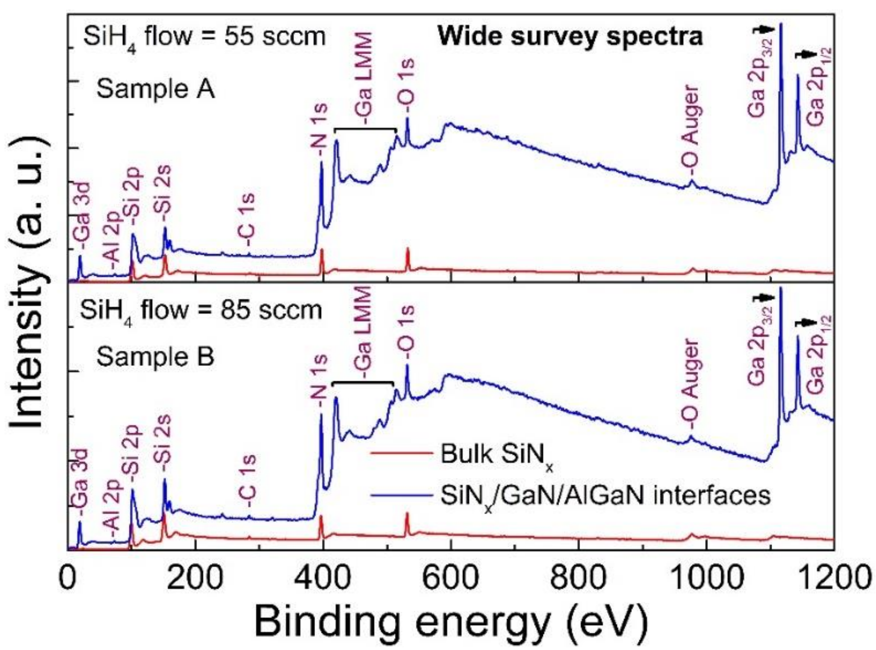

Fig. 4. Wide survey spectra obtained at the SiN_x/GaN/AlGaN interfaces and bulk SiN_x.

The deconvoluted Ga 3d and Si 2p narrow scan XPS spectra acquired at the SiN_x/GaN/AlGaN interfaces are portrayed in Fig. 5. Notably, the deconvoluted Ga 3d spectra reveal four different peaks associated with various chemical bonds. The major peaks in sample A can be designated as overlapped N 2s state at 17.32 ± 0.1 eV, Ga-Ga at 18.81 ± 0.1 eV, Ga-N at

19.7 ± 0.1 eV, and Ga^{3+}-O bonds at 20.45 ± 0.1 eV [35-38]. Interestingly, the Ga 3d core level spectrum in sample B is shifted about 0.9 eV towards the lower binding energy. The higher binding energy of the Ga 3d core level spectrum in sample A could be related to the formation of strong Ga-N bonds with the presence of higher NH_y radicals which might reduce the nitrogen vacancy in the GaN surface. On the other hand, the Ga-O bonds at higher binding energy reduce noticeably in sample B, implying that due to higher SiH_4 flow, the excess Si compensated with the pre-existed oxygen contamination on the surface [4]. Noted, in GaN-based devices, the Ga-O bond states may act as the deep-level surface traps and deteriorate the device performance strongly.

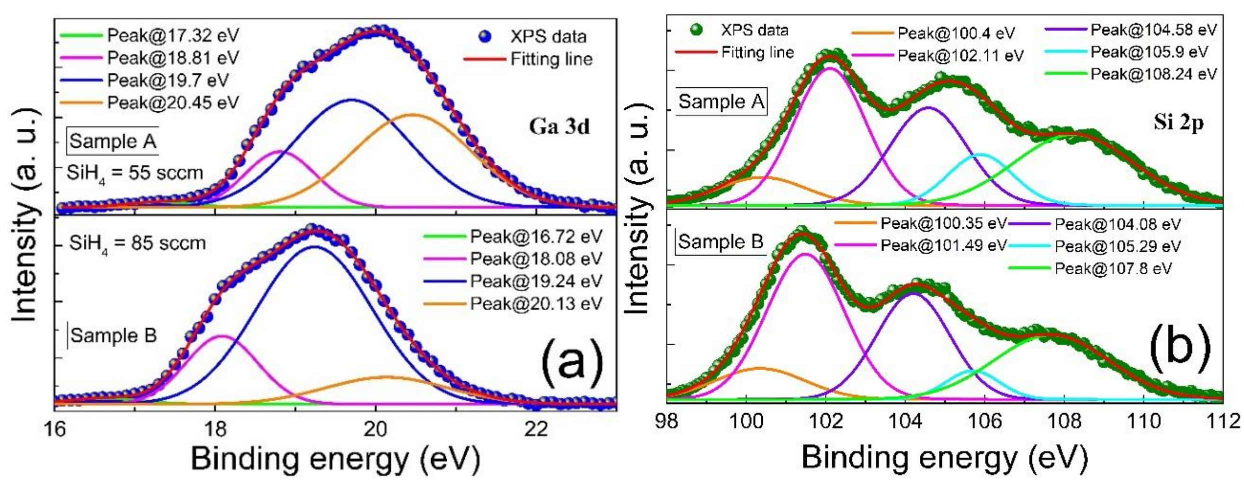

Fig. 5. XPS spectra of (a) Ga 3d and (b) Si 2p acquired at the SiN_x/GaN/AlGaN interfaces.

The variation of chemical bonds with SiH_4 flow can also be noticed in Si 2p core level spectra (Fig. 5 (b)). When the SiH_4 flow rate increases from 55 to 85 sccm, the contribution of Si-Si bonds at 100.35 eV and Si-N at 101.49 eV improves, expressing that higher SiH_4 content increases the availability of reactive Si species and enhances the interaction possibility between silicon and nitrogen. It can be noticed in Fig. 5 (b) that the Si-O bond density (peak at 101.49 eV with pink line) in sample B is higher (~14%) than that of sample A, indicating that the excess Si compensated quickly with the surface oxygen and formed the lower energy Si-O bonds [3,4]. The formation of Si-O bonds in sample B helps to decrease the density of Ga-O traps (peak at 105.29 eV) up to 13%. Additionally, the formation of strong Ga-N bonds in sample A (green line) with the presence of higher NH_y radicals can be found in the decomposed Si 2p spectra, suggesting that N-vacancy filled up more frequently with higher NH_3 content.

Additionally, the deposition of a thick passivation layer may help to reduce the interface states and improve the carrier transport in the device. Therefore, the impact of SiH_4 flow rate on the deposition of SiN_x insulating layer and the role of a passivation layer should be investigated step by step. This investigation can help to understand the dominating key factors that control the device performance critically. With this aim in mind, we have fabricated different MIS-diodes and measured different device characterizations at room temperature. The obtained results are thoroughly described in the subsequent sections.

3.4. I–V characteristics

The typical *I–V* characteristics of the fabricated conventional MS-diode and MIS-diodes are shown in Fig. 6. Both forward current and reverse leakage current decrease due to the insertion of PECVD-SiN_x layer as a gate insulator. After passivation, a further reduction in reverse leakage current is observed (see Fig. 6), implying the requirement of a thick passivation layer in the MIS-diode to mitigate the compelling effect of surface states. Nevertheless, in comparison to a conventional MS-diode, MIS-diode C and MIS-diode D exhibited 4.5×10^3 and 1.1×10^3 times lower magnitude of I_{leak} at -10 V, demonstrating that the higher SiH_4 flow (85 sccm) can control the interface properties of PECVD-SiN_x on GaN/AlGaN in a better way. The lowest value of I_{leak} in MIS-diode D suggests that the higher SiH_4 flow (85 sccm) prevents the formation of interface trap states (say for instance, N-H bonds) which are associated with the leakage processes, such as trap-assisted tunneling (TAT) at lower voltage regime or Frenkel–Poole emission (FPE) at higher voltage regime [27,39,40].

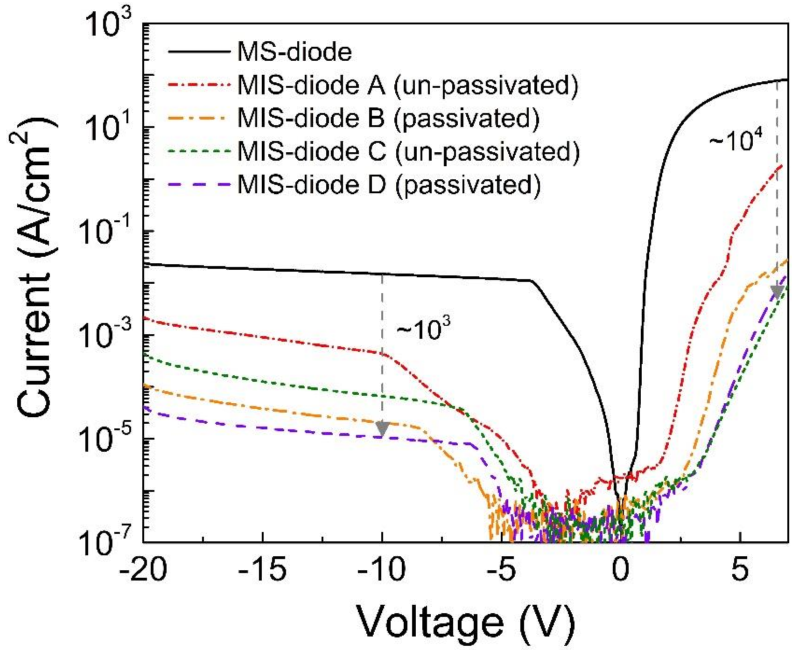

Fig. 6. Variation of gate leakage current in two terminal MS-diode and MIS-diodes as a function of bias voltage. The diameter of the circle diodes is 100 μm.

3.5. C-V characteristics

The room temperature *C-V* results of MS-diode and MIS-diodes are shown in Fig. 7. To explain the bias-dependent *C-V* characteristics*,* three different regions, namely, I, II, and III are specified in Fig. 7. In MIS-diode, a sharp decrease in capacitance is observed in region I (high reverse bias), demonstrating the complete depletion of 2DEG (pinch-off voltage of the SiN_x/GaN/AlGaN/GaN-based MIS-diode). In region II, the measured capacitance is almost constant due to the series capacitance of the barrier and SiN_x gate dielectric layer. The constant capacitance in region II implies that 2DEG exists at the AlGaN/AlN/GaN interface with a nearly constant density [41,42]. A step-like increase in capacitance at a higher forward bias (> 2 V, region III) is also observed, specifying the electron transfer from the AlGaN barrier to GaN/SiN_x interfaces.

As can be seen in region I, the depletion characteristics of 2DEG as a function of applied bias are altered not only with the SiH_4 flow rate but also after the inclusion of an additional passivation layer. Noted, the modification of the depletion characteristics of 2DEG (stretch-out of the *C–V* curves) is more prominent in MIS-diode A and B (un-passivated and passivated devices). In particular, MIS-diode A shows a partial depletion of 2DEG. This is ascribed to the presence of several electronic states near the 2DEG channel. The stretch-out of the *C–V* curves could be related to the existence of different discrete states (donor-type and/or acceptor-type at different locations) [41,43,44]. Such discrete states can act as a fixed charge state at the SiN_x/GaN/AlGaN interfaces and shift the *C–V* curve with respect to the applied bias [44]. In this bias region, the Fermi level should be located near the conduction band minimum of the AlGaN barrier. During the voltage sweep, the movement of E_F at the interface can strongly change the occupation of various interface states and affect the depletion capacitance in MIS-diode [41,43]. Based on the observation in Fig. 7, we surmised that the higher SiH_4 flow declines the defect states in the MIS-diode, leading to the control of E_F movement in a better way that can shrink the stretch-out behaviors of *C–V* curves.

In addition, the dielectric constant (ε) of the employed SiN_x layer can also be calculated from the *C–V* results as suggested in Refs. [45-48]. To calculate ε, we have used the following equation [47,48]

$$C_{MISdiode} = C_{Diode} \times \left[1 + \frac{d_{SiN}}{d_B} . \frac{\varepsilon_B}{\varepsilon_{SiN}}\right]^{-1} \tag{1}$$

where ε_B, ε_{SiN}, d_B, *and* d_{SiN} are the dielectric constant and thickness of the GaN/AlGaN barrier layer and SiN_x insulator layer, respectively.

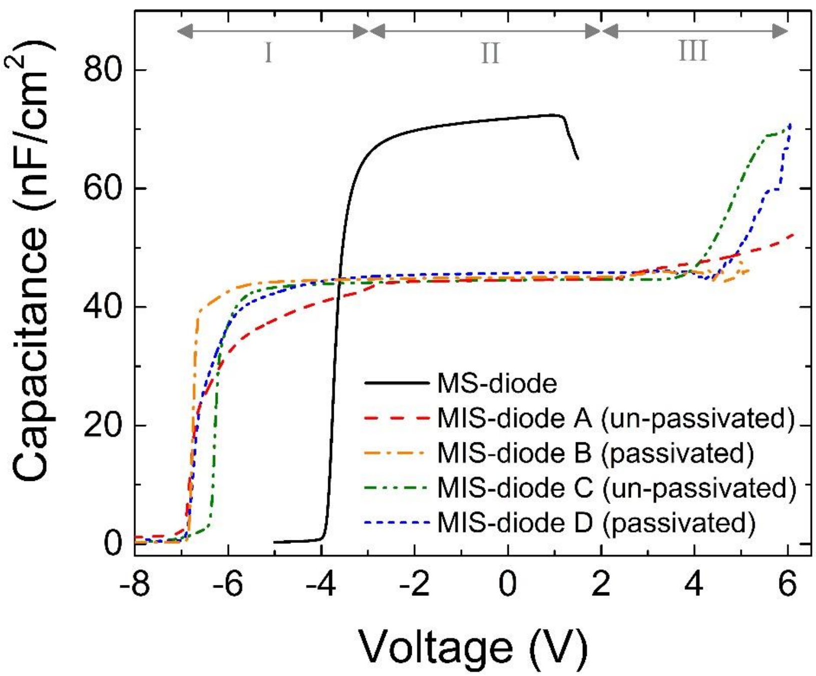

Fig. 7. *C–V* characteristics of two terminal MS-diode and MIS-diodes at 10 kHz.

From Fig. 7, we have estimated the capacitance density (C_{den}) at zero-bias of about 71.78, 44.51, and 44.53, nF/cm^2 for MS-diode and MIS-diode A, and B, respectively. Based on the obtained results, we have calculated the values of ε_{SiN} which are about 6.9 and 7.7 for MIS-diode A, and B, respectively. Park et al. have estimated ε_{SiN} ~ 7.5 in the Si-rich Si_xN film having a refractive index of 2.2 which agrees well with our results [45]. The higher value of Si/N ratio can increase the dielectric constant in SiN_x film noticeably suggested by the authors in Ref. [46]. Therefore, we believe the higher value of ε_{SiN} MIS-diode B is attributed to the improved Si/N composition. However, a quantitative analysis of interface-state density will help to understand the effect of SiH_4 flow on the charge transport property of the device which we thoroughly elucidate in the next section.

3.6. Frequency-dependent conductance measurements

To evaluate the interface-state density and trap time constant (τ_{it}) in the PECVD-SiN_x/GaN/AlGaN MIS-diodes, we performed the frequency-dependent conductance measurements at RT which are presented in Fig. 8 [13,48-50]. We have varied the frequency (f) from 1 kHz to 5 MHz to measure the conductance (G_m) at different bias voltages. When the applied bias approaches the pinch-off voltage of the MIS-diode, the Fermi level can be located within the bandgap of GaN layer which can help to capture the existing interface trap states [51]. The equivalent circuits for the SiN_x/GaN interface are presented in the inset of Fig. 8 (b) which we have considered to calculate the parallel conductance (G_p) [51,52]. The equivalent circuit (I) in the inset of Fig. 8 (b) can be transformed into a frequency-dependent capacitance (C_p) in parallel with the value of G_p, as presented in circuit (II). The circuit fitting parameters presented in the equivalent circuits can be calculated by the method described in Ref. [53]. With certain assumptions (details are available in Ref. [53]), we can estimate the fitting parameters for the investigated devices. For example, at high frequency, the values of C_S, C_{SiN}, and C_p in MIS-diode A are 72, 0.023, 8.1 nF/cm^2, whereas G_p is about 50.4 mS/cm^2.

The G_p/ω vs ω curves in MIS-diode A (un-passivated) show two distinct peaks with respect to the frequency, implying the presence of low-frequency and high-frequency trap levels at the interface of the device. Notably, in passivated MIS-diode B, the magnitude of the peaks associated with the interface traps, particularly at low-frequency (slow trap) is reduced. This is attributed to the improvement of interface properties with the passivation. However, when we increase the SiH_4 flow from 55 to 85 sccm in MIS-diode C (un-passivated), the magnitude of the peaks declines considerably. This result indicates that higher SiH_4 flow improves the interface properties by reducing N-H and Ga-O bonds as noticed in sections 3.2 and 3.3. Interestingly, the passivated MIS-diode D exhibits a single peak with a notably lower magnitude. This is ascribed to the lowering of trap levels at the interface.

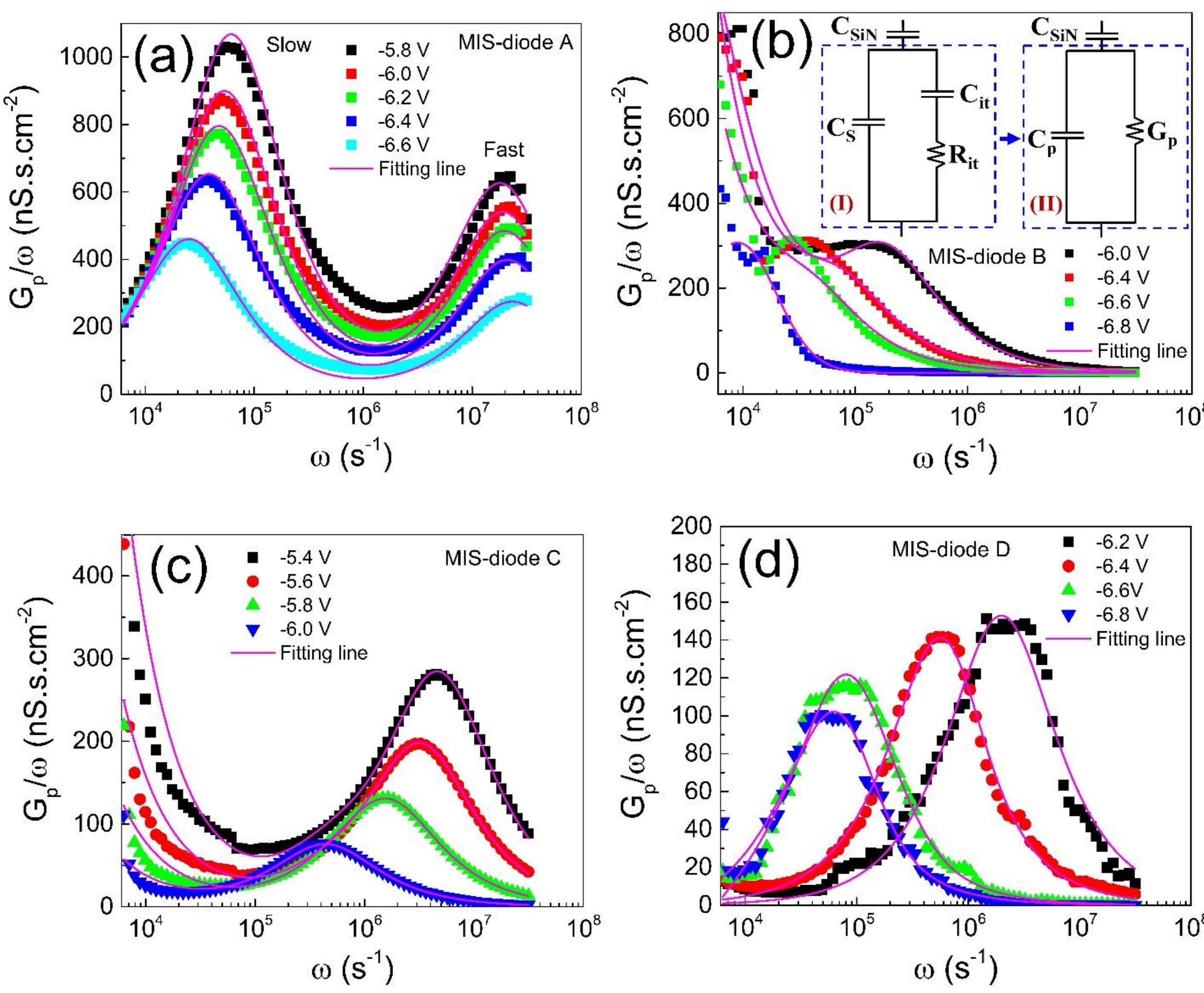

Fig. 8. Measured (solid points) and fitting ((solid lines)) curves of G_p/ω vs ω at different bias voltages for (a) MIS-diode A (un-passivated, SiH_4 flow = 55 sccm), (b) MIS-diode B (passivated, SiH_4 flow = 55 sccm), (c) MIS-diode C (un-passivated, SiH_4 flow = 85 sccm), and (d) MIS-diode D (passivated, SiH_4 flow = 85 sccm). Inset (in Fig. 8 (b)): (I) an equivalent RC circuit of MIS-diode with $\tau_{it} = C_{it}.R_{it}$, and (II) A simplified RC circuit used in parallel conductance-based D_{it} analysis.

The peak regions in the G_p/ω vs ω plots are associated with the interface traps. Different interface trap levels can be expressed as [13,48,52]

$$\frac{G_p}{\omega} = \frac{\omega C_{SiN}^2 G_m}{\omega^2 (C_m - c_{SiN})^2 + G_m^2} = \frac{q\omega D_{it1}\tau_1}{1+(\omega\tau_1)^2} + \frac{q\omega D_{it2}\tau_2}{1+(\omega\tau_2)^2} \quad (2)$$

where ω (= $2\pi f$) is the radial frequency, C_{SiN}^2 and C_m are the capacitance of the gate insulator and the measured capacitance at a frequency ω. Other parameters, namely, D_{it1}, D_{it2}, τ_1, and τ_2 are the interface trap densities and the time constants for slow and fast (high-frequency) traps, respectively.

The trap state energy level with respect to the conduction band can be determined using the following equation [13,48,52].

$$E_T = -kTln(\tau_{it} v_t \sigma_T N_C) \quad (3)$$

where T (= 300 K) is the temperature, v_t (= 2.6×10^7 cm.s^{-1}) is the thermal velocity of electrons, σ_T (= 3.4×10^{-15} cm^{-2}) is the electron capture cross-section, N_C (= $4.3 \times 10^{14} \times T^{3/2}$ cm^{-3}) is the effective density of states of GaN in the conduction band [13,48]. However, the experimental results in G_p/ω vs ω plots are fitted by using Eqs. (2) and (3) to calculate D_{it1}, D_{it2}, τ_1 and τ_2. A similar extraction method for such trap parameters has also been suggested in Refs. [13,48,52,54]. However, the extracted values of D_{it1}, D_{it2}, τ_1, and τ_2 are plotted as a function of interface state energy located at a depth of (E_C-E_T) in Fig. 9.

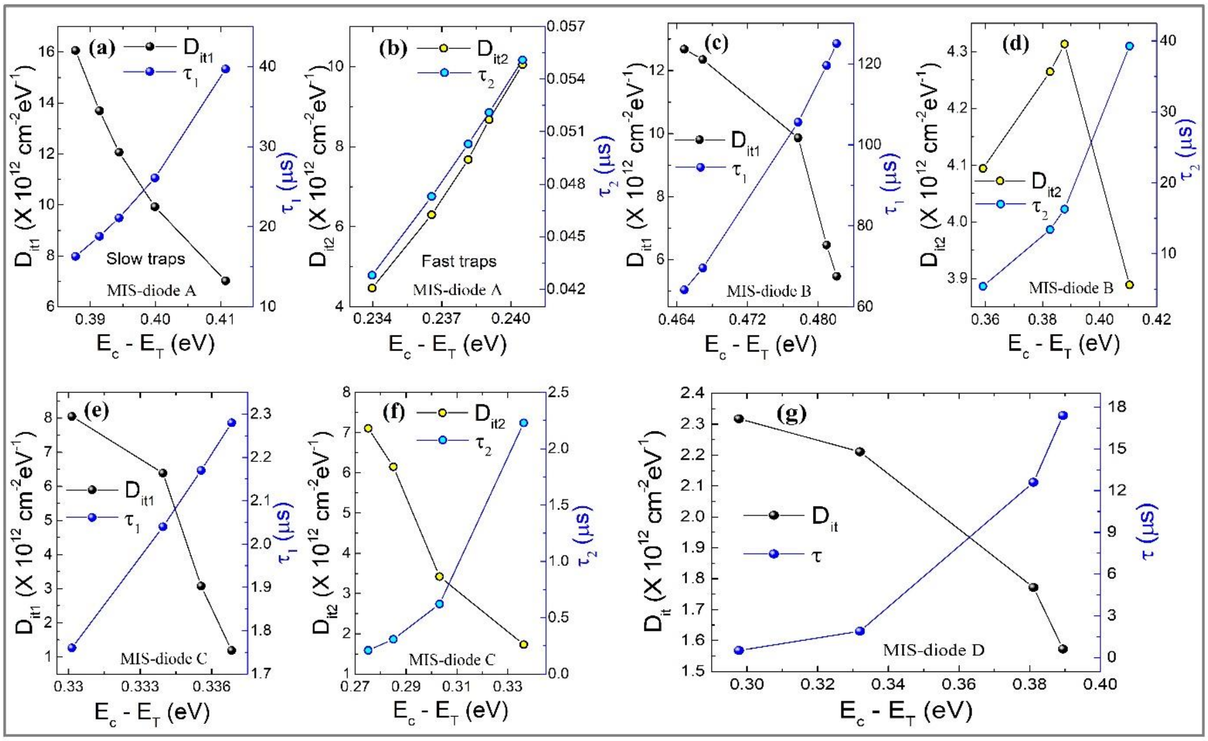

Fig. 9. Plots of D_{it} and τ_{it} as a function of interface state energy located at a depth of (E_C-E_T) for (a) MIS-diode A (un-passivated), (b) MIS-diode B (passivated), (c) MIS-diode C (un-passivated), and (d) MIS-diode D (passivated).

It is evident in Fig. 9 that in un-passivated devices, both D_{it1}, and D_{it2} are much lower in MIS-diode C compared to MIS-diode A. This is ascribed to the reduction of surface oxygen-related bonds with higher SiH_4 flow, improving the SiN_x/GaN interface. Furthermore, after passivation, the interface state density reduces considerably due to the enhancement in interface property. It is interesting to note that MIS-diode D exhibits a single peak only. This could be ascribed to the overlap of slow and fast trap states after passivation and thus the interface trap density in MIS-diode D is denoted as D_{it}. We believe the formation of a single peak with a slightly lower magnitude in MIS-diode D helps to improve the device performance. On the other hand, the combined effect of slow and fast traps is more effective in worsening the device performance as noticed above. However, in the present work, we have achieved a minimum D_{it} of 1.57×10^{12} cm^{-}

^{2}.eV^{-1} at 0.389 eV in MIS-diode D which is comparable to those of the reported state-of-the-art PECVD-SiN_x/GaN/AlGaN/GaN MIS-diodes (see the benchmarking in Table 1). This significantly lower interface state density in MIS-diode D could be attributed to the lower surface pinning effect compared to the other devices. It is noted that a larger surface pinning effect can improve the barrier lowering in the heterostructures and boost the surface state-related conduction process [54,55]. The lower surface pinning effect and lower electronic states help to reduce the leakage current largely in MIS-diodes B and D [56]. Additionally, as the voltage increases, both D_{it1}, and D_{it2} decline mostly as the trap levels go more deeper into the bandgap. From the trends of the variation of D_{it} with E_C-E_T, we have surmised that both slow and fast traps are not uniformly distributed in the interface [13]. However, the reduction in the interface trap density in different MIS-diodes with respect to MIS-diode A is noted in Table 2.

Trap time constants (slow and fast) in the ingestigated devices increase with increasing voltage. This change in time constants is related to trapping and de-trapping mechanisms. If both trapping and de-trapping processes have existed during the carrier transport, the trap time constant can be defined as $\tau^{-1} = \tau_t^{-1} + \tau_e^{-1}$ (τ_t is the tunneling time; τ_e ($1/2\pi f$) is the emission time related to the de-trapping process) [56,57]. It is suggested that the electric field in the wide bandgap AlGaN barrier can be decreased with the applied bias voltage, which in turn prolongs the carrier tunneling time and improves τ_t in the device [56,57]. The higher SiH_4 flow for the gate dielectric helps to reduce the trap time constant by avoiding the formation of Ga-O bonds, leading to a smaller leakage current in the device as noticed in Fig. 6. In addition, the time constant in passivated devices is slightly higher than that of un-passivated devices. This could be either related to the shift of G_p/ω peaks toward the lower characteristic frequency where the fast traps can superimpose with slow trap states (called redistribution of trap states) or the enhancement of de-trapping process

[58,59]. The widening of peaks as noticed in Fig. 8 could be ascribed to the redistribution of traps, expanding the span time of carriers at the trap centers. However, to get more information about the inherent mechanism of the various trap states having different energies and time constants, further research is required.

Table 1 Benchmarking of the minimum interface trap density ($D_{it\text{-}min}$) and E_c-E_T ($E_{t\text{-}min}$) in PECVD-SiN_x/GaN MIS-diodes.

Insulator/ Process	Thickness (nm)	Deposition temperature	Epilayer	$E_{t\text{-}min}$ (eV)	$D_{it\text{-}min}$ ($cm^{-2}\ eV^{-1}$)	Ref.
SiN/PECVD	-	-	AlGaN/GaN on SiC	0.3-0.35	3.7×10^{13}	[60]
SiN_x/PECVD	78	300 °C	AlGaN/AlN/GaN on SiC	0.3-0.4	1.3×10^{13}	[42]
SiN_x/PECVD	30	-	AlGaN/GaN on Si	0.3-0.39	3×10^{12}	[14]
SiN_x/PECVD	22	-	AlN/AlGaN/GaN on Si	0.304-0.482	3×10^{12}	[58]
SiN/PECVD	20	400 °C	GaN/AlGaN/GaN on Si	-	1.2×10^{12}	[61]
SiN_x/PECVD	20	300 °C	AlGaN/GaN on Si	0.406-0.452	1.0×10^{12}	[54]
SiN_x/PECVD	100	300 ºC	*n*-GaN	-	6.5×10^{11}	[62]
SiN_x/PECVD	20	300 ºC	GaN/AlGaN/GaN on diamond	0.27-0.36	4×10^{11}	[59]
SiN_x/PECVD	11	300 °C	GaN/AlGaN/GaN on Si	0.298-0.389	1.57×10^{12}	[This work]

Table 2 The estimated values of $D_{it2\text{-}min}$ in different MIS-diodes.

Device	$D_{it2\text{-}min}$ ($\times 10^{12}\ cm^{-2}\ eV^{-1}$)	Reduction in $D_{it2\text{-}min}$ (%)*
MIS-diode A (un-passivated)	4.47	-
MIS-diode B (passivated)	3.89	13
MIS-diode C (un-passivated)	1.73	61
MIS-diode D (passivated)	1.57	65

*All reductions are calculated with respect to MIS-diode A

4. Conclusion

The deposition of PECVD-SiN_x gate insulator and passivation layers with higher SiH_4 flow appears to have two influential effects, namely, improved interface properties through the modification of chemical structures at the interface during the deposition and excellent surface passivation quality of the GaN. Ellipsometry results suggest that the refractive index of SiN_x film increases from 2.05 to 2.26 with the increase of SiH_4 flow rate from 55 to 85 sccm, indicating the increase of Si-Si absorbing bonds in the deposited SiN_x film. On the other hand, several interface trap states related to Ga-O and N-H bonds decrease due to higher SiH_4 flow as confirmed via XPS and FTIR measurements. We obtained a significantly lower value of I_{leak} in MIS-diode C compared to MIS-diode A, implying that the improved interface properties with higher SiH_4 flow assist in decreasing the value of I_{leak}. The lowering of interface electronic states in the MIS-diode with higher SiH_4 flow might control the E_F movement in a better way and shrink the observed stretch-out behaviors of *C–V* curves. Additionally, the higher value of dielectric constant evaluated from the *C–V* results in MIS-diode B compared to MIS-diode A is attributed to the larger Si/N ratio in the gate insulator layer. Finally, after passivation, the trap densities, especially the slow traps are suppressed strongly, and we achieved a minimum D_{it} of 1.57×10^{12} cm^{-2}.eV^{-1} in MIS-diode D which is also helping to suppress three orders of lower magnitude I_{leak} compared to the conventional MS-diode.

CRediT authorship contribution statement

Pradip Dalapati: Conceptualization, Device fabrication, Characterizations, Data curation, Investigation, Methodology, Validation, Writing—original draft, Writing—review and editing. **Subramaniam Arulkumaran:** Conceptualization, Data curation, Validation, Writing – review & editing. **Dinesh Mani:** Device fabrication, Formal analysis. **Hanchao Li:** Device fabrication, Formal analysis. **Hanlin Xie:** Conceptualization, Device fabrication, Formal analysis. **Yue Wang:** Device fabrication, Formal analysis. **Geok Ing Ng:** Conceptualization, Data curation, Methodology, Funding acquisition, Resources, Supervision, Validation, Writing—review and editing, Coordinated the work and contributed to manuscript review.

Declaration of Competing Interest

The authors declare that they have no known competing financial interests or personal relationships that could have appeared to influence the work reported in this paper.

Data availability

Data will be made available on reasonable request from the corresponding author.

Acknowledgements

This research/project is supported by A*STAR under the RIE2025 Manufacturing, Trade, and Connectivity Programmatic Fund (Award M21K6b0134). The authors would like to thank Dr. S. Das (School of Material Science and Engineering, NTU) for his assistance in the XPS and FTIR measurement and data analysis.

References

[1] P. Gamarra, C. Lacam, M. Tordjman, F. Medjdoub, M.A. di Forte-Poisson, In-situ passivation of quaternary barrier InAlGaN/GaN HEMTs, J. Cryst. Growth 464 (2017) 143–147, http://dx.doi.org/10.1016/j.jcrysgro.2016.11.014.

[2] D.Y. Chen, A.R. Persson, K.H. Wen, D. Sommer, J. Grünenpütt, H. Blanck, M. Thorsell, O. Kordina, V. Darakchieva, P.O.A. Persson, J.T Chen, N. Rorsman, Impact of *in situ* NH_3 pre-treatment of LPCVD SiN passivation on GaN HEMT performance, Semicond. Sci. Technol. 37 (2022) 035011, https://doi.org/10.1088/1361-6641/ac4b17.

[3] J. Liu, M. Mi, J. Zhu, S. Liu, P. Wang, Y. Zhou, Q. Zhu, M. Wu, H. Lu, B. Hou, H. Wang, X. Cai, Y. Zhang, X. Duan, L. Yang, X. Ma, Y. Hao, Improved power performance and the mechanism of AlGaN/GaN HEMTs using Si-rich SiN/Si_3N_4 bilayer passivation, IEEE Trans. Electron Devices 69 (2022) 631–636, https://doi.org/10.1109/TED.2021.3133822.

[4] J. Long Liu, J. Jie Zhu, M.H. Mi, Q. Zhu, S.Y. Liu, P.F. Wang, Y.W. Zhou, Z.Y. Zhao, J.D. Zhou, M. Zhang, M. Wu, B. Hou, H. Wang, L. Yang, X.H. Ma, Y. Hao, 8.7 W/mm output power density and 42% power-added-efficiency at 30 GHz for AlGaN/ GaN HEMTs using Si-rich SiN passivation interlayer, Appl. Phys. Lett. 120 (2022) 052101, https://doi.org/10.1063/5.0080120.

[5] S. Ardali, F. Sonmez, S.B. Lisesivdin, T. Malin, V. Mansurov, K. Zhuravlev, E. Tiras, The comprehensive investigation of barrier layers on power loss mechanisms in AlGaN/GaN HEMT structures, Mater. Sci. Eng. B 300 (2024) 117075, https://doi.org/10.1016/j.mseb.2023.117075.

[6] B. Mounika, J. Ajayan, Sandip Bhattacharya, 2.5 A/mm/350 GHz aggressively scaled gate engineered Fe-doped AlN/ GaN channel HEMT with graded InGaN Backbarrier on SiC-wafer for next generation RF power electronics applications, Mater. Sci. Eng. B 301 (2024) 117194, https://doi.org/10.1016/j.mseb.2024.117194.

[7] A. Kumar, M. Kumar, R. Kaur, A.G. Joshi, S. Vinayak, R. Singh, Barrier height enhancement of Ni/GaN Schottky diode using Ru based passivation scheme, Appl. Phys. Lett. 104 (2014) 133510, http://dx.doi.org/10.1063/1.4870624.

[8] L. Shen, X. Cheng, Z. Wang, C. Xia, D. Cao, L. Zheng, Q. Wang, Y. Yu, Passivation effect of graphene on AlGaN/GaN Schottky diode, RSC Adv. 5 (2015) 86593, https://doi.org/10.1039/c5ra12550b.

[9] A. Kumar, T. Singh, M. Kumar, R. Singh, Sulphide passivation of GaN based Schottky diodes, Curr. Appl. Phys. 14 (2014) 491–495, http://dx.doi.org/10.1016/j.cap.2013.12.021.

[10] P. Dalapati, S. Urata, T. Egawa, Investigation of AlGaN/GaN high electron mobility transistors on Silicon (111) substrates employing multi-stacked strained layer superlattice structures, Superlattice. Microst. 147 (2020) 106709, https://doi.org/10.1016/j.spmi.2020.106709.

[11] V.K. Surana, S. Ganguly, D. Saha, Performance improvement in AlGaN/GaN high-electron-mobility transistors by low-temperature inductively coupled plasma–chemical vapor deposited SiN_x as gate dielectric and surface passivation, Phys. Status Solidi A 219 (2022) 2200509, https://doi.org/10.1002/pssa.202200509.

[12] S. Zhang, K. Wei, Y.C. Zhang, X.J. Chen, S. Huang, H.B. Yin, G.G. Liu, T.T. Yuan, Y.K. Zheng, X.H. Wang, X.Y. Liu, Well-suppressed interface states and improved transport properties of AlGaN/GaN MIS-HEMTs with PEALD SiN gate dielectric, Vacuum 191 (2021) 110359, https://doi.org/10.1016/j.vacuum.2021.110359.

[13] M. Whiteside, S. Arulkumaran, Y. Dikme, A. Sandupatla, G.I. Ng, Improved interface state density by low temperature epitaxy grown AlN for AlGaN/GaN metal-insulator-semiconductor diodes, Mater. Sci. Eng. B 262 (2020) 114707, https://doi.org/10.1016/j.mseb.2020.114707.

[14] X. Gao, H. Guo, R. Wang, D. Pan, P. Chen, D. Chen, H. Lu, R. Zhang, Y. Zheng, Low Leakage current and high breakdown field AlGaN/GaN MIS-HEMTs using PECVD-SiN_x as a gate dielectric, Micromachines 13 (2022) 1396, https://doi.org/10.3390/mi13091396.

[15] Y. Hong, X. Zheng, Y. He, K. Liu, H. Zhang, X. Wang, Z. Yuan, F. Zhang, Y. Wang, X. Ma, Y. Hao, Enhancing performance of β-Ga_2O_3 diodes through a $Ni_xO/SiN_x/Ga_2O_3$ sandwich structure, J. Alloy. Compd. 976 (2024) 173062, https://doi.org/10.1016/j.jallcom.2023.173062.

[16] X. Lu, K. Yu, H. Jiang, A. Zhang, and K. M. Lau, Study of interface traps in AlGaN/GaN MISHEMTs using LPCVD SiN_x as gate dielectric, IEEE Trans. Electron Devices 64 (2017) 824, https://doi.org/10.1109/TED.2017.2654358.

[17] R. Chaudhuri, A. Hickman, J. Singhal, J. Casamento, H.G. Xing, D. Jena, In situ crystalline AlN passivation for reduced RF dispersion in strained-channel AlN/GaN/AlN high-electron-mobility transistors, Phys. Status Solidi A 219 (2022) 2100452, https://doi.org/10.1002/pssa.202100452.

[18] A. Siddique, R. Ahmed, J. Anderson, M. Holtz, E.L. Piner, Improved electrical properties of AlGaN/GaN high-electron-mobility transistors by in situ tailoring the SiN_x passivation layer, ACS Appl. Mater. Interfaces 13 (2021) 18264−18273, https://doi.org/10.1021/acsami.1c01241.

[19] Y. Yamaguchi, K. Nakamura, H. Ohmi, H. Kakiuchi, K. Yasutake, Investigation of structural properties of high-rate deposited SiN*x* films prepared at low temperatures (100–300 °C) by atmospheric-pressure plasma CVD, Phys. Status Solidi C 7 (2010) 824–827, https://doi.org/10.1002/pssc.200982693.

[20] Z. Chen, M. Mi, J. Liu, P. Wang, Y. Zhou, M. Zhang, X. Ma, Y. Hao, A novel Si-rich SiN bilayer passivation with thin-barrier AlGaN/GaN HEMTs for high performance millimeter-wave applications, Chin. Phys. B 31, 117105 (2022), https://doi.org/10.1088/1674-1056/ac81a6.

[21] E.A. Douglas, P. Mahony, A. Starbuck, A. Pomerene, D.C. Trotter, C.T. Derose, Effect of precursors on propagation loss for plasma-enhanced chemical vapor deposition of SiN_x:H waveguides, Opt. Mater. Express 6 (2016) 2892–2903, http://dx.doi.org/10.1364/OME.6.002892.

[22] Y. Wan, K.R. McIntosh, A.F. Thomson, Characterisation and optimisation of PECVD SiN_x as an antireflection coating and passivation layer for silicon solar cells, AIP Adv. 3 (2013) 032113, http://dx.doi.org/10.1063/1.4795108.

[23] F. Massines, J. Silva, J.F. Lelievre, R. Bazinette, J. Vallade, P. Lecouvreur, S. Pouliquen, Hydrogenated silicon nitride SiN_x:H deposited by dielectric barrier discharge for photovoltaics, Plasma Process. Polym. 13 (2016) 170–183, http://dx.doi.org/10.1002/ppap.201500182.

[24] J.F. Lelievre, E. Fourmond, A. Kaminski, O. Palais, D. Ballutaud, M. Lemiti, Study of the composition of hydrogenated silicon nitride SiN_x:H for efficient surface and bulk passivation of silicon, Sol. Energy Mater. Sol. Cells 93 (2009) 1281–1289, http://dx.doi.org/10.1016/j.solmat.2009.01.023.

[25] M. Ghaderi, R.F. Wolffenbuttel, Design and fabrication of ultrathin silicon-nitride membranes for use in UV-visible airgap-based MEMS optical filters, Journal of Physics: Conference Series 757 (2016) 012032, http://dx.doi.org/10.1088/1742-6596/757/1/012032.

[26] H.H. Nguyen, R. Jayapal, N.S. Dang, V.D. Nguyen, T.T. Trinh, K. Jang, J. Yi, Investigation of charge storage and retention characteristics of silicon nitride in NVM based on InGaZnO channels for System-on-Panel applications, Microelec. Eng. 98 (2012) 34–40, http://dx.doi.org/10.1016/j.mee.2012.05.058.

[27] S. Zhang, K. Wei, Y. Xiao, X.H. Ma, Y.C. Zhang, G.G. Liu, T.M. Lei, Y.K. Zheng, S. Huang, N. Wang, M. Asif, X.Y. Liu, Effect of SiN:H_x passivation layer on the reverse gate leakage current in GaN HEMTs, Chin. Phys. B 27 (2018) 097309, http://dx.doi.org/10.1088/1674-1056/27/9/097309.

[28] R. Baby, A. Venugopalrao, H. Chandrasekar, S. Raghavan, M. Rangarajan D.N. Nath, Study of the impact of interface traps associated with SiN_x passivation on AlGaN/GaN MIS-HEMTs, Semicond. Sci. Technol. 37 (2022) 035005, https://doi.org/10.1088/1361-6641/ac48dd.

[29] H. Mackel, R. Ludemann, Detailed study of the composition of hydrogenated SiN_x layers for high-quality silicon surface passivation, J. Appl. Phys. 92 (2002) 2602–2609, https://doi.org/10.1063/1.1495529.

[30] G. Scardera, T. Puzzer, G. Conibeer, M.A. Green, Fourier transform infrared spectroscopy of annealed silicon-rich silicon nitride thin films, J. Appl. Phys. 104 (2008) 104310, https://doi.org/10.1063/1.3021158.

[31] I. Guler, Optical and structural characterization of silicon nitride thin films deposited by PECVD, Mater. Sci. Eng. B 246 (2019) 21–26, https://doi.org/10.1016/j.mseb.2019.05.024.

[32] D, Das, C. Patra, Wide optical gap B-doped nc-Si thin films with advanced crystallinity and conductivity on transparent flexible substrates for potential low-cost flexible electronics including nc-Si superstrate p–i–n solar cells, Mater. Adv. 2 (2021) 2055, https://doi.org/10.1039/d0ma00915f.

[33] P. Dalapati, K. Yamamoto, T. Kubo, T. Egawa, M. Miyoshi, Bias-controlled photocurrent generation process in GaN-based ultraviolet p–i–n photodetectors fabricated with a thick Al_2O_3 passivation layer, Optik 245 (2021) 167691, https://doi.org/10.1016/j.ijleo.2021.167691.

[34] P. Dalapati, K. Yamamoto, T. Egawa, M. Miyoshi, Evaluation of high-performance, self-powered and wavelength-selective InGaN/GaN multiple quantum well UV photodetectors fabricated on sapphire substrate: Analysis of the influence of growth temperature, Sens. Actuators A Phys. 331 (2021) 113050–113060, https://doi.org/10.1016/j.sna.2021.113050.

[35] M. Grodzicki, J.G. Rousset, P. Ciechanowicz, E. Piskorska-Hommel, D. Hommel, XPS studies on the role of arsenic incorporated into GaN, Vacuum 167 (2019) 73–76, https://doi.org/10.1016/j.vacuum.2019.05.043.

[36] R. Wasielewski, M. Grodzicki, J. Sito, K. Lament, P. Mazur, A. Ciszewski, Ru/GaN(0001) interface properties, Acta Phys. Pol 132 (2017) 354–356, https://doi.org/10.12693/APhysPolA.132.354.

[37] J. Yanagisawa, M. Toda, T. Kitamura, H. Matsumoto, Y. Akasaka, Formation of GaN layer on SiN surface using low-energy Ga ion implantation, J. Vac. Sci. Technol. B 23 (2005) 3205–3208, https://doi.org/10.1116/1.2134722.

[38] A.J. Tzou, K.H. Chu, I.F. Lin, E. Ostreng, Y.S. Fang, X.P. Wu, B.W. Wu, C.H. Shen, J.M. Shieh, W.K. Yeh, C.Y. Chang, H.C. Kuo, AlN surface passivation of GaN-based high electron mobility transistors by plasma-enhanced atomic layer deposition, Nanoscale Res. Lett. 12 (2017) 315, https://doi.org/10.1186/s11671-017-2082-0.

[39] B.S. Eller, J.Yang, R.J. Nemanich, Electronic surface and dielectric interface states on GaN and AlGaN, J. Vac. Sci. Technol. A 31 (2013) 050807, https://doi.org/10.1116/1.4807904.

[40] Y. Yan, V. Kilchytska, B. Wang, S. Faniel, Y. Zeng, J.P. Raskin, D. Flandre, Characterization of thin Al_2O_3/SiO_2 dielectric stack for CMOS transistors, Microelec. Eng. 254 (2022) 111708, https://doi.org/10.1016/j.mee.2022.111708.

[41] C. Mizue, Y. Hori, M. Miczek, T. Hashizume, Capacitance–voltage characteristics of Al_2O_3/AlGaN/GaN structures and state density distribution at Al_2O_3/AlGaN interface, Jpn. J. Appl. Phys. 50 (2011) 021001–021007, https://doi.org/10.1143/JJAP.50.021001.

[42] M. Fagerlind, F. Allerstam, E.Ö. Sveinbjörnsson, N. Rorsman, A. Kakanakova-Georgieva, A. Lundskog, U. Forsberg, E. Janzén, Investigation of the interface between silicon nitride passivations and AlGaN/AlN/GaN heterostructures by C(V) characterization of metal-insulator-semiconductor-heterostructure capacitors, J. Appl. Phys. 108 (2010) 014508, https://doi.org/10.1063/1.3428442.

[43] M. Miczek, B. Adamowicz, C. Mizue, T. Hashizume, Simulations of capacitance–voltage–temperature behavior of metal/insulator/AlGaN and metal/insulator/AlGaN/GaN structures, Jpn. J. Appl. Phys. 48 (2009) 04C092–04C096, https://doi.org/10.1143/JJAP.48.04C092.
[44] M. Miczek, C. Mizue, T. Hashizume, B. Adamowicz, Effects of interface states and temperature on the C-V behavior of metal/insulator/AlGaN/GaN heterostructure capacitors, J. Appl. Phys. 103 (2008) 104510, https://doi.org/10.1063/1.2924334.
[45] D.G. Park, M. Tao, D. Li, A.E. Botchkarev, Z. Fan, Z. Wang, S.N. Mohammad, A. Rockett, J.R. Abelson, H. Morkoç, A.R. Heyd, S.A. Alterovitz, Gate quality Si_3N_4 prepared by low temperature remote plasma enhanced chemical vapor deposition for III–V semiconductor-based metal–insulator–semiconductor devices, J. Vac. Sci. Technol. B 14 (1996) 2674–2683, https://doi.org/10.1116/1.589003.
[46] K.D. Vargheese, G.M. Rao, Electrical properties of silicon nitride films prepared by electron cyclotron resonance assisted sputter deposition, J. Vac. Sci. Technol. A 19 (2001) 2122–2126 (2001), https://doi.org/10.1116/1.1374631.
[47] M.J. Anand, G.I. Ng, S. Vicknesh, S. Arulkumaran, K. Ranjan, Reduction of current collapse in AlGaN/GaN MISHEMT with bilayer SiN/Al_2O_3 dielectric gate stack, Phys. Status Solidi C 10 (2013) 1421–1425, https://doi.org/10.1002/pssc.201300219.
[48] M. Whiteside, S. Arulkumaran, G.I. Ng, Demonstration of vertically-ordered h-BN/AlGaN/GaN metal-insulator-semiconductor high-electron-mobility transistors on Si substrate, Mater. Sci. Eng. B. 270 (2021) 115224, https://doi.org/10.1016/j.mseb.2021.115224.
[49] S. Yang, Z. Tang, K.Y. Wong, Y.S. Lin, Y. Lu, S. Huang, K.J. Chen, Mapping of interface traps in high-performance Al_2O_3/AlGaN/GaN MIS-heterostructures using frequency- and temperature-dependent C-V techniques, 2013 IEEE International Electron Devices Meeting, (2013), https://doi.org/10.1109/IEDM.2013.6724573.
[50] M. Whiteside, S. Arulkumaran, Y. Dikme, A. Sandupatla, G.I. Ng, Demonstration of AlGaN/GaN MISHEMT on Si with low-temperature epitaxy grown AlN dielectric gate, Electronics 9 (2020) 1858, https://doi.org/10.3390/electronics9111858.
[51] S. Liu, S. Yang, Z. Tang, Q. Jiang, C. Liu, M. Wang, B. Shen, K.J. Chen, Interface/border trap characterization of Al_2O_3/AlN/GaN metal-oxide-semiconductor structures with an AlN interfacial layer, Appl. Phys. Lett. 106 (2015) 051605, https://doi.org/10.1063/1.4907861.
[52] A. Rawat, M. Meer, V.K. Surana, N. Bhardwaj, V. Pendem, N.S. Garigapati, Y. Yadav, S. Ganguly, D. Saha, Thermally Grown TiO_2 and Al_2O_3 for GaN-Based MOS-HEMTs, IEEE Trans. Electron Devices 65 (2018) 3725–3731, https://doi.org/10.1109/TED.2018.2857468.
[53] S.M. Sze, K.K. Ng, Physics of semiconductor devices, John Wiley & Sons, Inc., Hoboken, New Jersey, third edition, (2007) p. 213–219.
[54] R. Baby, A. Venugopalrao, H. Chandrasekar, S. Raghavan, M. Rangarajan, D.N. Nath, Study of the impact of interface traps associated with SiN_x passivation on AlGaN/GaN MIS-HEMTs, Semicond. Sci. Technol. 37 (2022) 035005, https://doi.org/10.1088/1361-6641/ac48dd.

[55] Z. Zhang, M. Hua, J. He, G. Tang, Q. Qian, K.J. Chen, Ab initio study of impact of nitridation at amorphous-SiN_x/GaN interface, Appl. Phys. Express 11 (2018) 081003, http://dx.doi.org/10.7567/APEX.11.081003.

[56] J.J. Zhu, X.H. Ma, B. Hou, W.W. Chen, Y. Hao, Investigation of trap states in high Al content AlGaN/GaN high electron mobility transistors by frequency dependent capacitance and conductance analysis, AIP Adv. 4 (2014) 037108, http://dx.doi.org/10.1063/1.4869020.

[57] P. Zhang, S.L. Zhao, J.S. Xue, J.J. Zhu, X.H. Ma, J.C. Zhang, Y. Hao, Investigation of trap states in Al_2O_3 InAlN/GaN metal–oxide–semiconductor high-electron-mobility transistors, Chin. Phys. B 24 (2015) 127306, http://dx.doi.org/10.1088/1674-1056/24/12/127306.

[58] Y. Lu, Q. Jiang, Z. Tang, S. Yang, C. Liu, K.J. Chen, Characterization of SiN_x/AlN passivation stack with epitaxial AlN grown on AlGaN/GaN heterojunctions by plasma-enhanced atomic layer deposition, Appl. Phys. Express 8 (2015) 064101, http://dx.doi.org/10.7567/APEX.8.064101.

[59] K. Ranjan, S. Arulkumaran, G.I. Ng, A. Sandupatla, Low interface trap density in AlGaN/GaN metal–insulator–semiconductor high-electron-mobility transistors on CVD-diamond, 2020 4th IEEE Elect. Dev. Tech. Manufac. Con. (EDTM), pp. 1–4 (2020), http://dx.doi.org/10.1109/EDTM47692.2020.9117851.

[60] W.H. Wu, Y.H. Lin, C.K. Lin, F.H. Huang, W.C. Wang, Investigation of un-doped GaN cap layer on RF and trap related characteristics in AlGaN/GaN HEMTs, available at https://csmantech.org/wp-content/uploads/Digest/Digests-2021/5.2.2021-CS-MANTECH_Final-Paper_Wen-Hsin-Wu.pdf (accessed on 29th Jan 2024).

[61] L.Q. Zhang, P.F. Wang, AlGaN/GaN HEMT with LPCVD deposited SiN and PECVD deposited SiCOH low-k passivation, Appl. Phys. Express 12 (2019) 036501, https://doi.org/10.7567/1882-0786/ab0139.

[62] S. Arulkumaran, T. Egawa, H. Ishikawa, T. Jimbo, M. Umeno, Investigations of SiO_2/*n*-GaN and Si_3N_4/*n*-GaN insulator–semiconductor interfaces with low interface state density, Appl. Phys. Lett. 73 (1998) 809–811, https://doi.org/10.1063/1.122009.